

www.acsabm.org Article

Fabrication of Rhenium Disulfide/Mesoporous Silica Core-Shell Nanoparticles for a pH-Responsive Drug Release and Combined **Chemo-Photothermal Therapy**

Ha Na, Jake Carrier, Samuel Oyon, and Cheng-Yu Lai*



Cite This: ACS Appl. Bio Mater. 2024, 7, 3337-3345



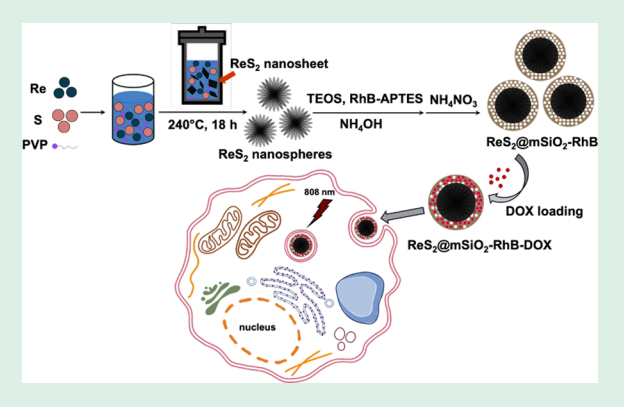
ACCESS I

III Metrics & More

Article Recommendations

Supporting Information

ABSTRACT: A stimuli-responsive drug delivery nanocarrier with a core-shell structure combining photothermal therapy and chemotherapy for killing cancer cells was constructed in this study. The multifunctional nanocarrier ReS₂@mSiO₂-RhB entails an ReS₂ hierarchical nanosphere coated with a fluorescent mesoporous silica shell. The three-dimensional hierarchical ReS₂ nanostructure is capable of effectively absorbing nearinfrared (NIR) light and converting it into heat. These ReS₂ nanospheres were generated by a hydrothermal synthesis process leading to the selfassembly of few-layered ReS₂ nanosheets. The mesoporous silica shell was further coated on the surface of the ReS₂ nanospheres through a surfactant-templating sol-gel approach to provide accessible mesopores for drug uploading. A fluorescent dye (Rhodamine B) was covalently attached to silica precursors and incorporated during synthesis in the mesoporous silica walls toward conferring imaging capability to the



nanocarrier. Doxorubicin (DOX), a known cancer drug, was used in a proof-of-concept study to assess the material's ability to function as a drug delivery carrier. While the silica pores are not capped, the drug molecule loading and release take advantage of the pH-governed electrostatic interactions between the drug and silica wall. The ReS₂@mSiO₂-RhB enabled a drug loading content as high as 19.83 mg/g doxorubicin. The ReS2@mSiO2-RhB-DOX nanocarrier's cumulative drug release rate at pH values that simulate physiological conditions showed significant pH responsiveness, reaching 59.8% at pH 6.8 and 98.5% and pH 5.5. The in vitro testing using HeLa cervical cancer cells proved that ReS₂@mSiO₂-RhB-DOX has a strong cancer eradication ability upon irradiation with an NIR laser owing to the combined drug delivery and photothermal effect. The results highlight the potential of ReS₂@mSiO₂-RhB nanoparticles for combined cancer therapy in the future.

KEYWORDS: rhenium disulfide, mesoporous silica, doxorubicin, drug release, chemo-photothermal therapy

1. INTRODUCTION

Cancer is a ubiquitous health problem and is responsible for more than 16% of deaths worldwide. Chemotherapy, used alone or combined with radiation therapy, remains the main treatment modality for cancer treatment being the most effective approach to eradicate tumors. However, due to equal impact on both cancerous and noncancerous cells, as well as drugs' wide distribution after systemic administration, chemotherapy renders multiple side effects and can be ultimately toxic to patients.² To improve the efficacy of cancer treatment, combining two or more therapies governed by different mechanisms is another promising strategy.³ One of the treatments combined with chemotherapy is hyperthermia, which has been demonstrated to directly induce the death of cancer cells or increase their sensitivity to other therapeutic methods.⁴ Nanocarrier-based drug delivery systems present promising alternative approaches that also enable the combination of various therapies and have been shown to significantly enhance the therapeutic efficacy of active drugs. In

contrast to chemotherapy, nanoparticles benefit from precise targeting, along with long-term stability and biocompatibility.⁵ Furthermore, nanocarriers that generate thermal responses upon application of external stimuli have been demonstrated to overcome the limitations of traditional hyperthermia, in which the temperature indiscriminately increases in both healthy tissues and the target tissue. Literature reports confirm that gold, iron, copper, tungsten, molybdenum, and carbon-based nanomaterials can serve as heat carriers that can convert infrared light into cytotoxic heat under near-infrared light irradiation. 6-11 When these photothermal agents are used in

Received: February 29, 2024 Revised: April 25, 2024 Accepted: April 30, 2024 Published: May 3, 2024





combination with chemotherapy, the cytotoxicity of many chemotherapeutic drugs is significantly enhanced at elevated temperatures, often resulting in a synergistic effect. ¹² However, phototherapeutic agents are not typically designed to carry drugs, requiring the simultaneous delivery of the drug at the target site by an independent carrier. The prospect of combining different materials with dissimilar physicochemical properties in a unique entity that could accomplish both functions remains of great interest in the field of nanomedicine. ¹³

Among materials with the potential to function as hybrid nanostructures for this purpose, two-dimensional (2D) nanomaterials have become important candidates due to their layered structures and unique optical properties. 14,15 Twodimensional (2D) transition metal dichalcogenides (2D TMDCs) are graphene-like nanomaterials with biological toxicity significantly lower than that of graphene, providing a large surface area to accommodate guest molecules, including chemotherapy drugs such as doxorubicin (DOX). Recent reports demonstrated that polyethylene glycol (PEG)-coated MoS₂ can efficiently load DOX and exhibit promising synergistic photothermal and chemotherapy efficacy in tumor cells both in vitro and in vivo. 16 Similarly, WS₂ nanosheets coated with a mesoporous silica shell showed that loading with DOX triggered its intracellular release via NIR-induced photothermal heating and enhanced cancer cell killing.

Another well-known TMDC, rhenium disulfide (ReS₂), is an effective radiopharmaceutical nanoagent that has been applied in *in vivo* tumor radiation therapy as well as in radiation synovectomy. Moreover, rhenium disulfide has shown significant near-infrared absorption and high photothermal conversion efficiency (PTCE) when applied in clinical studies. However, to the best of our knowledge, there are no reports on ReS₂-based hybrid nanoplatforms applied in combined photothermal and stimuli-responsive drug delivery therapeutics.

Herein, we prepared ReS₂ with spherical morphology through a bottom-up hydrothermal method using a modified literature procedure.²⁰ The unique morphology of ReS₂ is ascribed to the formation of nanoobjects with a quasi-spherical geometry and a porous 3D framework by in situ self-assembly of small ReS₂ nanosheets. The obtained ReS₂ nanospheres showed good photothermal capabilities, as expected for ReS2. To fabricate the multifunctional core-shell nanoparticles (ReS₂@mSiO₂-RhB), the nanospheres were further coated with mesoporous silica via solution-phase deposition. Doxorubicin (DOX) was used to test the drug uploading and release capacity of the ReS2@mSiO2-RhB. Upon DOX encapsulation, ReS₂@mSiO₂-RhB-DOX was exposed to acidic pH, which triggered the drug release. In vitro testing in HeLa cell culture revealed that ReS₂@mSiO₂-RhB-DOX can successfully enter cells through endocytosis, and given the acidic endosomal pH (~ 5.5) , it released the DOX inside the cells. Therefore, we anticipate that this strategy has potential in chemo/PTT combined therapy toward tumor eradication.

2. MATERIALS AND METHODS

2.1. Chemicals. Tetraethyl orthosilicate (TEOS, 99.9%) was procured from Alfa Aesar (Haverhill, MA) and hexadecyltrimethylammonium bromide (CTAB, ≥99%) was from Sigma-Aldrich (Saint Louis, MI). Ammonium hydroxide solution (NH₄OH, 28% NH₃ basis), hydrochloric acid (HCl, 37%), thiourea (99%), ammonium perrhenate (VII) (NH₄ReO₄, 99+%), ammonium nitrate (NH₄NO₃,

99+%), and methanol were procured from ThermoFisher Scientific (Waltham, MA). ACS reagent-grade nanopure water was purchased from LabChem (Zelienople, PA), and ethanol (200 proof, 100% by volume) from Decon Laboratories (King of Prussia, PA). Doxorubicin hydrochloride was procured from TCI America (Portland, OR). The cell culture medium (Gibco Dulbecco's Modified Eagle Medium (DMEM), Cytiva HyClone Calf Serum, and penicillin—streptomycin (Pen/Strep 10,000 U/mL) were purchased from ThermoFisher (Waltham, MA, USA), and Dulbecco's phosphate-buffered saline (DPBS, pH 7.4) without calcium and magnesium was purchased from Lonza Bioscience (Walkersville, MD). The Cell Counting Kit-8 (CCK-8) was procured from GLPBIO Technology Inc. (Montclair, CA, USA). The green nucleic acid stain BD Via-Probe was procured from BD (Franklin Lakes, NJ). All chemicals were used as received without any further purification (unless otherwise indicated).

2.2. Characterization. X-ray powder diffraction (XRD) measurements were performed on a Rigaku MiniFlex600 equipped with Cu $K\alpha$ radiation ($\lambda = 1.5405 \text{ Å}$) operated at 40 mV and 30 mA to validate the presence of the ReS2. Fourier transform infrared spectroscopy (FT-IR) was conducted on a Shimadzu/IRTracer-100 to confirm the surfactant template removal. Dynamic light scattering measurements were performed at room temperature on a Malvern/Zetasizer Nano-ZSZEN3600 instrument. Particle size and morphology were evaluated by TEM nanoparticle imaging, performed with a JEOL JEM-2100Plus instrument. The JEOL JEM-2100Plus is equipped with EDS (energy dispersive spectroscopy), which enabled elemental mapping. The materials' specific surface areas were determined via nitrogen adsorption-desorption isothermal curves using the Brunauer-Emmett-Teller (BET) theory. The density functional theory (DFT) method was employed for determining the materials' pore volume and pore size distribution. These analyses were performed on an Anton Paar Quantachrome/NOVAtouch LX-2 instrument. UVvis absorption spectroscopy was employed using a UV-visible spectrophotometer (Thermo Scientific/BioMate 160). Raman spectroscopy was performed with a confocal Raman microscope (WITec alpha300 R) using a 532 nm laser. Fluorescence imaging was performed using an Invitrogen EVOS M7000 confocal laser scanning imaging system. BioTEM imaging of HeLa cells was performed with a Thermo Scientific Talos L120C transmission electron microscope employing standard room temperature methods. The photothermal therapy study was conducted with a 808 nm NIR laser (RLDH808-1200-5, Roithner Laserthchnik Gmbh, Vienna, Austria). A TH-5 Thermalert Clinical Monitoring Thermometer (Physitemp Instruments, Clifton, NJ) was utilized to record the solution temperature. The cell culture plates were kept at 37 °C using a heated stage insert (World Precision Instruments Inc.).

2.3. Synthesis of ReS₂. ReS₂ nanospheres were synthesized by a facile hydrothermal method. ²⁰ In a typical experiment, 1.0 mmol of ammonium perrhenate (NH₄ReO₄, 268.24 mg), 4.5 mmol of thiourea (NH₂CSNH₂, 342.54 mg), and 10.5 mmol of polyvinylpyrrolidone (PVP, MW \approx 55,000, 580 mg) were dissolved in 30 mL of nanopure water under magnetic stirring. Upon complete dissolution of all reactants, the resulting solution was transferred into a 50 mL Teflonlined stainless-steel autoclave, which was heated in a furnace to 240 °C and kept at this temperature for 18 h. Next, the autoclave was allowed to cool naturally to room temperature, and the as-prepared material was collected by centrifugation and washed with water and ethanol three times. Upon drying, the resulting black powders were dried under vacuum overnight.

- **2.4. RhB (Rhodamine B) and APTES Conjugation.** The preparation followed a slightly modified published procedure. In a typical experiment, 0.01 mmol of RhB-ITC (5.00 mg) was dissolved in 9.8 mL of ethanol under magnetic stirring. After 10 min, 0.09 mmol of APTES (20 μ L) was added to the resulting homogeneous solution, and the mixture was continuously stirred overnight. The solution was kept in the dark until further use.
- **2.5.** Synthesis of Core-Shell ReS₂@mSiO₂-RhB Nanospheres. The silica shell of the core-shell ReS₂@mSiO₂-RhB nanospheres was prepared according to the Stöber method. First, a CTAB solution was prepared by mixing CTAB (0.30 g, 0.823)

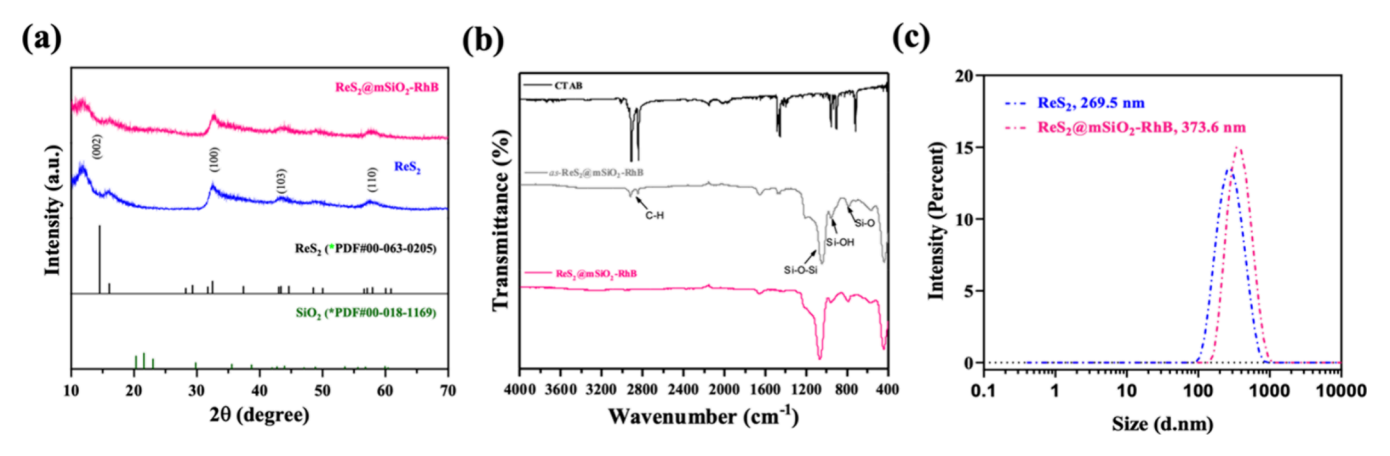


Figure 1. (a) XRD patterns of ReS₂ and ReS₂@mSiO₂-RhB, (b) FT-IR spectrum of as-ReS₂@mSiO₂-RhB and ReS₂@mSiO₂-RhB, and (c) DLS particle size measurements of ReS₂ and ReS₂@mSiO₂-RhB.

mmol), ethanol (30 mL), deionized water (80 mL), and ammonium hydroxide solution (1.00 g, 28 wt %). Separately, 0.10 g of assynthesized ReS2 nanospheres were dispersed in 30 mL of ethanol by ultrasonication. After 30 min, the dispersion was added to the previously prepared CTAB solution, and the resulting mixture was stirred for 30 min to form a uniform dispersion. A mixture of 0.40 g of TEOS (1.90 mmol) and 0.17 g of RhB-APTES conjugate solution as prepared above (Section 2.4) was added dropwise to this dispersion with continuous stirring. After 6 h, the product was collected by centrifugation and washed repeatedly with water and ethanol to remove any byproducts. Finally, the purified nanospheres (~0.2 g) were redispersed in a mixture of ethanol (60 mL, 95%) and ammonium nitrate (0.40 g) at room temperature for 6 h to remove the CTAB template. The successful removal of CTAB was verified by Fourier transform infrared (FT-IR) spectroscopy. The product was washed with ethanol to result in the final ReS2@mSiO2-RhB

2.6. Photothermal Performance of ReS2@mSiO2-RhB. The process followed a slightly modified published procedure.²³ The ReS2@mSiO2-RhB was dispersed in nanopure water at different concentrations (0, 10, 25, 50, 100, 150, 200, 250, and 300 μ g/mL). Then, 300 μ L for each concentration were dispensed in triplicate in a 96-well plate following by irradiation with an 808 nm NIR laser (Roithner Lasertechnik GmbH/RLDH808-1200-5) for 10 min in ambient conditions. The laser power density was 1 W/cm². The dispersion temperature was recorded every 30 s using a digital thermometer (Physitemp/TH-5) that was connected to a hightemperature microprobe thermocouple. The ReS₂@mSiO₂-RhB dispersion with 100 μ g/mL concentration was selected for measurements' repeatability evaluation, using the same procedure. The sequence of photothermal conversion and natural cooling measurements was repeated for five cycles to demonstrate the photothermal conversion repeatability of the ReS2@mSiO2-RhB dispersion. The calculation of the photothermal conversion efficiency followed previously reported methods.2

2.7. In Vitro Biocompatibility of ReS₂@mSiO₂-RhB. HeLa cells were seeded in a 96-well plate at 1×10^4 cells/well and incubated for 24 h before starting the treatments, using Dulbecco's Modified Eagle Medium (DMEM) supplemented with 10% calf serum and 1% Pen/Strep as the growth medium. The cells were then treated with varying concentrations (0, 10, 25, 50, 100, 150, 200, 250, and 300 μ g/mL) of ReS₂@mSiO₂-RhB. Cell viability 24 h post-transfection was assessed with a Cell Counting Kit-8 (CCK-8). The kit employs a water-soluble tetrazolium salt which is reduced by dehydrogenases in living cells to give a formazan product, with concentration directly proportional with the number of viable cells. Thus, measurement of the optical density values, conducted at a wavelength of 450 nm where formazan absorbs, reflects the number of viable cells.

The cells without any treatment served as a control. Briefly, the CCK-8 solution was mixed with the culture medium at a volume ratio

of 1:10, and 110 μL of the mixture was added to each well; the plates were then incubated at 37 $^{\circ}C$ for 2 h. Cells containing only CCK-8 solution and medium were set as a blank. The absorbance of all samples was measured at 450 nm using a microplate reader. The cell viability was obtained by using the following formula:

cell viability (%) = (OD test
$$-$$
 OD blank)/(OD control $-$ OD blank) \times 100%

2.8. Drug Loading of ReS₂@mSiO₂-RhB. Briefly, an amount of 100 mg of ReS₂@mSiO₂-RhB nanospheres was dispersed into 2 mL of PBS followed by the addition of 2 mg of DOX to achieve a final concentration of 1 mg/mL. The mixture was stirred at room temperature for 24 h. The unbound excess DOX was then removed by centrifugation, and the nanospheres were repeatedly washed with PBS. Each supernatant was collected, and the amount of DOX in the supernatant was determined by the absorbance peak of DOX at 480 nm, using a calibration curve. DOX loading efficiency was calculated with the following equation:

drug loading = [initial DOX (mg) - DOX in the supernatant
$$(mg)$$
]/nanosphere weight (mg)

2.9. Drug Release of $ReS_2@mSiO_2$ -RhB. A 10 mg portion of $ReS_2@mSiO_2$ -RhB-DOX was dispersed in 2 mL of PBS with different pH values (5.5, 6.8, and 7.4, respectively). The samples were placed and kept at 37 °C in an incubator. At predetermined time intervals, the samples, prepared in triplicate for each pH group, were centrifuged at 10,000 rpm, and 1.0 mL of the supernatant solution was collected from each sample followed by replacement with 1.0 mL of PBS in each sample. The UV-visible absorbance of each supernatant solution was measured with a spectrophotometer at 480 nm, and the release rate of DOX was calculated according to a standard curve for DOX concentration (Supporting Information).

2.10. Cell Viability. HeLa cells were seeded in a 96-well plate at 1×10^4 cells/well and incubated for 12 h. The cells were then treated with varying concentrations (0, 25, 50, 100, and 150 μ g/mL) of either ReS₂@mSiO₂-RhB, DOX, or ReS₂@mSiO₂-RhB-DOX (with a DOX loading of 19.83 mg/g) for 4 h, respectively. The excess materials were removed by rinsing three times with PBS. Culture medium was then added to the wells. The cells were subsequently exposed to an 808 nm laser at an output power density of 1 W/cm² for 10 min for photothermal treatment and incubated again at 37 °C with 5% CO₂ for 24 h. Afterward, the CCK-8 assay was tested to evaluate the cell viability. The measurements were taken in triplicate for each treatment group.

2.11. CLSM of Viable Cell Nucleic Acid Stain for HeLa Cells. HeLa cells were seeded in a 96-well plate with a concentration of 1×10^4 cells/well and incubated for 12 h before starting the treatments. The cells were then treated with 150 μ g/mL ReS₂@mSiO₂-RhB or

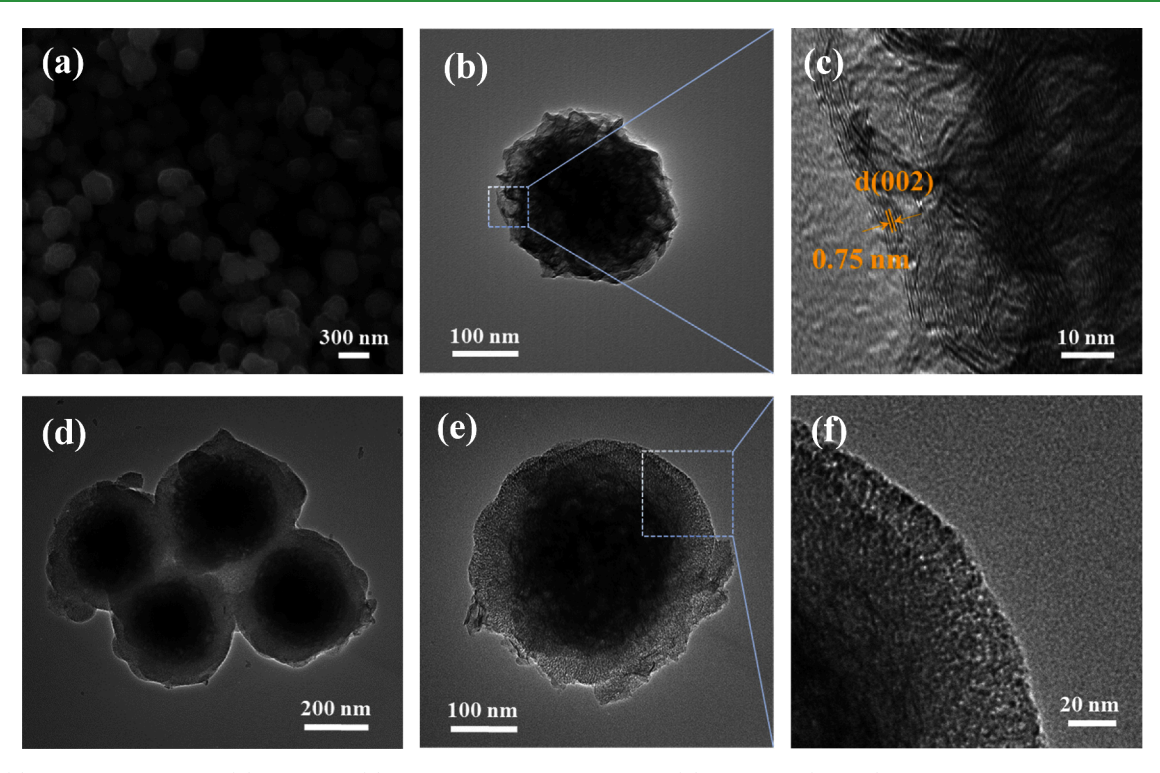


Figure 2. (a) SEM image of ReS2, (b) TEM and (c) HR-TEM images of ReS2, and (d) TEM and (e and f) HR-TEM images of ReS2@mSiO2-RhB.

ReS₂@mSiO₂-RhB-DOX (with a DOX loading of 19.83 mg/g) for 4 h. The cells were rinsed three times with PBS to remove any unbound nanospheres, and a culture medium was then added to the wells. The cells were subsequently exposed to an 808 nm laser at an output power density of 1 W/cm² for 10 min for photothermal treatment and incubated again at 37 °C with 5% CO₂ for 24 h. Afterward, 4% paraformaldehyde was used to fix the cells, and 0.5 μ M green nucleic acid stain (BD Via-Probe) was used to stain the viable cells. Finally, the living cells were imaged using an Evos confocal laser scanning fluorescence microscope with a 10x objective.

2.12. Statistical Analysis. The collected data were tabulated and the mean \pm standard deviation (SD) was calculated for each data set. For each experimental group, a two-way analysis of variance (ANOVA) followed by Tukey's post hoc test was conducted, by which p < 0.05 (*), p < 0.01 (***), p < 0.001 (****), and p < 0.0001 (****) were regarded as statistically significant.

3. RESULTS AND DISCUSSION

3.1. Characterization of ReS₂@mSiO₂-RhB. The powder XRD patterns in Figure 1a show that all reflections of ReS2 match the standard triclinic ReS2 structure (PDF#00-063-0205), indicating both crystallinity and purity.²⁴ Meanwhile, ReS₂ shows a broadened (002) diffraction peak that is significantly shifted from the standard peak position of 14.52° of ReSe₂ to 11.75°, revealing the increased interlayer distance of the (002) plane from 0.609 to 0.752 nm (calculated from the Bragg equation), matching well the HR-TEM results discussed below.²⁰ These results indicate that the porous ReS₂ nanospheres retain the triclinic ReS2 structure, while the interlayer distance is greatly expanded. The ReS₂@mSiO₂-RhB powder diffraction shows an intact structure of the ReS₂ in the hybrid ReS₂@mSiO₂-RhB, indicated by the overlapping ReS₂ peaks. The low-angle XRD exhibits mesoporous silica signature peaks in the nanosphere shell (Figure S1).

The removal of the CTAB template and the identification of the silica framework (Figure 1b) were validated by FT-IR spectroscopy. The peaks located at 2926 and 2854 cm⁻¹ are

the C-H stretching vibration peaks of methyl and methylene groups of CTAB, ²⁵ and the C-N stretching vibration peak at 1471 cm⁻¹ is the as-synthesized product, which no longer exists in the final product, proving that the CTAB template was successfully removed through the surfactant removal procedure. The peaks at about 1057, 964, and 789 cm⁻¹ are attributed to the stretching vibrations of Si-O-Si, Si-OH, and Si-O, respectively, in both spectra. ²⁶

The size and morphology of the ReS₂ and ReS₂@mSiO₂-RhB core-shell hybrid structures were evaluated by DLS, SEM, and TEM. A high-resolution transmission electron microscope (HR-TEM) was conducted to further observe the detailed structure. The dynamic light scattering (DLS) results (Figure 1c) show that the average diameters of the ReS₂ and ReS₂@mSiO₂-RhB nanospheres are 269.5 and 373.6 nm, respectively. Based on the SEM image in Figure 2a, ReS2 exhibits spherical shapes with corrugated surfaces; the size distribution plot in Figure S2 shows an average size distribution around 223.5 nm. The above electron microscope results are basically consistent with the DLS particle sizes. The TEM image in Figure 2b further validates the nanoparticles' uniform and spherical morphology, where the ReS2 nanospheres appeared to have formed from a random assembly of wavy few-layered ReS₂ nanosheets.²⁰ Furthermore, the HR-TEM in Figure 2c shows distances between adjacent layers with values of \sim 0.75 nm corresponding to the (002) plane. ^{20,28} The ReS₂@mSiO₂-RhB exhibits spherical core—shell structures with particle sizes of 300-400 nm as imaged by TEM (Figures 2d and 2e). Furthermore, the HR-TEM of ReS₂@mSiO₂-RhB proves the presence of the mesoporous silica shell of 40-60 nm in thickness (Figure 1f). In the SAED pattern of the ReS₂@ mSiO₂-RhB (Figure S3), the observed 'd' values are in agreement with those obtained from the ReS₂ XRD result.²⁹ The observed 'd' values of 0.74 nm also demonstrate the

ACS Applied Bio Materials www.acsabm.org Article

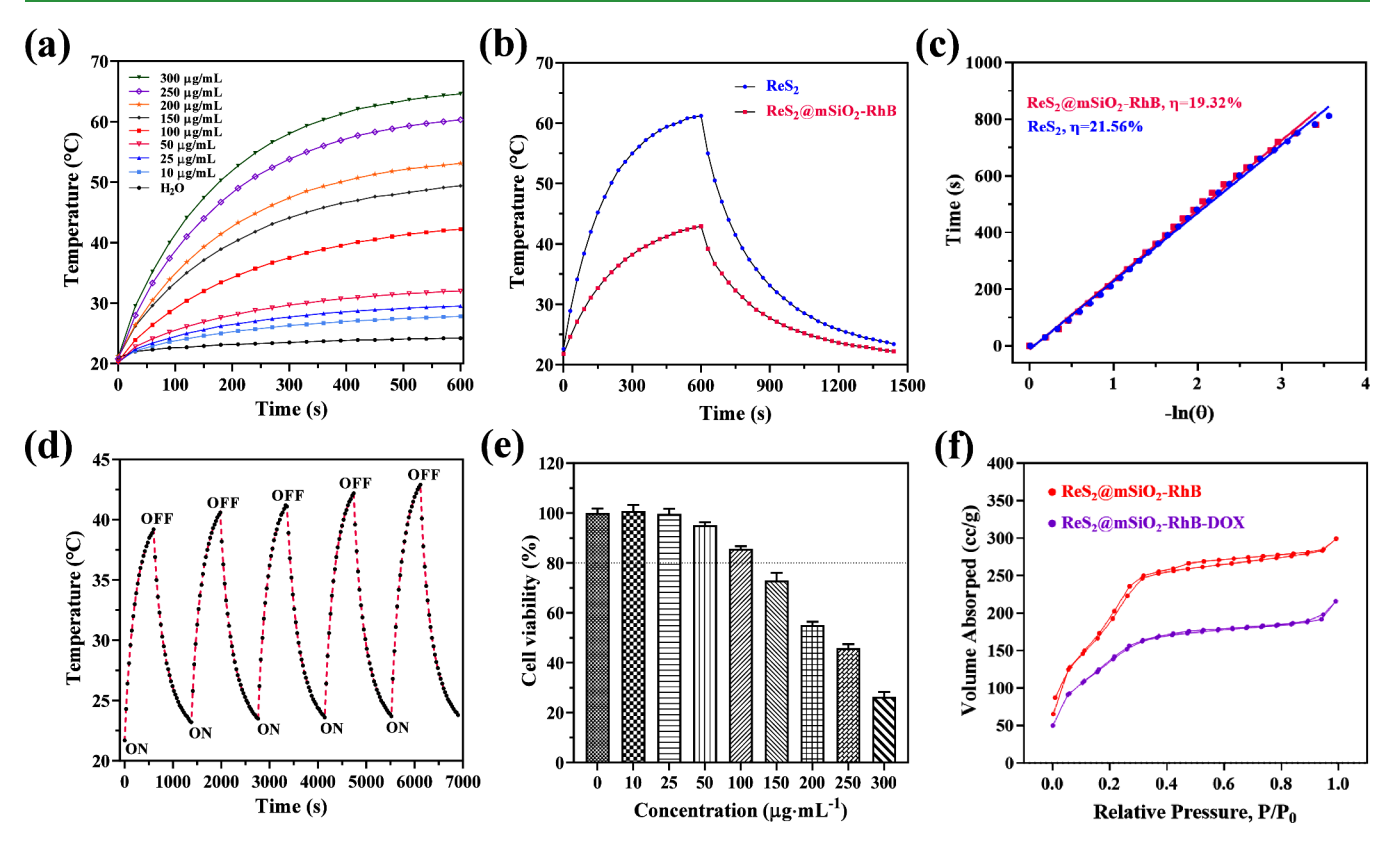


Figure 3. (a) Photothermal heating curves of ReS₂@mSiO₂-RhB dispersions at varied concentrations when irradiated by an 808 nm laser (1 W/cm², 10 min); (b) the temperature responses of ReS₂ (100 μ g/mL) and ReS₂@mSiO₂-RhB (100 μ g/mL) to the heating and cooling period; (c) plots of linear fitting time versus negative natural logarithm of driving force temperature (θ , see the Supporting Information); (d) photothermal stability of ReS₂@mSiO₂-RhB upon five cycles of laser irradiation; (e) cytotoxicity ReS₂@mSiO₂-RhB of after 24 h of incubation in HeLa cells; and (f) N₂ adsorption—desorption isotherm of ReS₂@mSiO₂-RhB and ReS₂@mSiO₂-RhB-DOX.

expanded layers of the ReS_2 (002) plane manifested in the shifted peaks in XRD.

3.2. In Vitro Photothermal Performance of ReS2@ mSiO₂-RhB. To verify the photothermal effect of ReS₂@ mSiO2-RhB, nanoparticles' dispersions at different concentrations were illuminated with an NIR laser (808 nm, 1 W/ cm²); quantitative analysis results are shown in Figure 3a. The results reveal that the dispersion temperature increased with the irradiation time, and the higher the concentration, the higher the temperature, which are observations consistent with the ReS₂ infrared irradiation results in Figure S4a. At a selected fixed concentration (100 µg/mL) the ReS₂@mSiO₂-RhB dispersion was sequentially exposed to NIR for 10 min and then cooled at room temperature. At this concentration, the ReS₂@mSiO₂-RhB dispersion temperature rapidly rises from 21.8 to 42.9 °C, while the ReS₂ dispersion temperature can rise from 22.6 to 61.2 °C (Figure 3b). The figure of merit for photothermal activity is photothermal conversion efficiency (η) . The calculated η using our previously reported method² revealed that the photothermal conversion efficiency of the core—shell ReS₂@mSiO₂-RhB (19.32%) is slightly smaller than that of ReS₂ (21.56%), as illustrated in Figure 3c. As shown in Figure 3d, the photothermal stability of ReS₂@mSiO₂-RhB was also measured under the above-fixed concentration; the dispersion was tested for five on and off switching cycles, and the results indicated that ReS2@mSiO2-RhB has good photostability. The slight temperature increase is perceived as the cycle number increases, which is ascribed to a minimal evaporation occurring in sequentially exposed solution; hence,

a slight increase of the nanospheres concentration corresponds to the decrease in the total volume of heated dispersion under near-infrared irradiation.

3.3. *In Vitro* Biocompatibility of ReS₂@mSiO₂-RhB. Determining the biocompatibility of ReS₂@mSiO₂-RhB is important for advancing its applicability in biomedical applications. As shown in Figure 3e, the material biocompatibility is investigated using the CCK-8 assay in HeLa cells. Following 24 h incubation with ReS₂@mSiO₂-RhB, the viability of HeLa cells remained >80% at concentrations below 100 μ g/mL. These results demonstrate that at low concentrations, ReS₂@mSiO₂-RhB has good *in vitro* biocompatibility.

3.4. ReS₂@mSiO₂-RhB Drug Loading. The mesoporous silica shell pore structure of ReS₂@mSiO₂-RhB facilitates the encapsulation of drug molecules. DOX molecules were loaded into ReS₂@mSiO₂-RhB via simple electrostatic adsorption from a PBS solution, with a DOX concentration of 1 mg/mL. The nanospheres were then separated by centrifugation, and the supernatant was subjected to UV–vis spectrophotometry measurements at λ_{480} nm to quantify loading. For the used DOX concentration of 1 mg/mL, the drug loading content reached 19.83 mg/g (Figure S5).

To further evaluate the loading, BET-specific surface area measurements were conducted for the $ReS_2@mSiO_2$ -RhB porous hybrid material. In Figure 3f, the nitrogen sorption isotherm of $ReS_2@mSiO_2$ -RhB reveals a type IV(c) isotherm showing type H4 hysteresis consistent with IUPAC specifications. The BET-specific surface area (Figure S6a) of $ReS_2@$

 $mSiO_2$ -RhB was calculated as 866 m^2/g . The pore size distribution curve (Figure S6b) originates from the adsorption data based on the density functional theory (DFT) method.

Following DOX loading, the isotherm shows a type II character, which is consistent with pore blockage/filling with the drug, leading to a more microporous character. Furthermore, the BET-specific surface area (Figure S6c) of $ReS_2@mSiO_2$ -RhB was calculated as 338 m²/g, which is small in comparison to the preloading surface area. The pore size distribution curve derived from the adsorption data (Figure S6d) shows that the average pore size is significantly reduced. The peak of the pore structure is relatively weakened because the ability of the small pores in the thin layer of the silica shell to absorb N_2 becomes smaller, indicating that most of the pore structure is filled with DOX.

3.5. ReS₂@mSiO₂-RhB-DOX Drug Release Study. The pH-responsive drug release of ReS₂@mSiO₂-RhB-DOX was evaluated at 37 °C under different pH conditions. The pH values of 7.4, 6.8, and 5.5 were selected corresponding to physiological pH, tumor microenvironment, and intracellular endosome, respectively.³¹ As shown in Figure 4, at pH 7.4, the

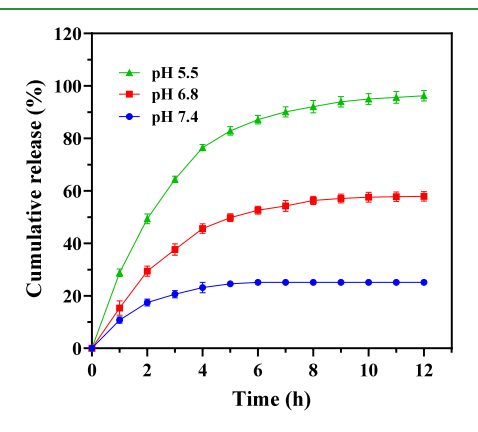


Figure 4. Drug release profiles for $ReS_2@mSiO_2$ -RhB-DOX in 12 h at different pH conditions (pH = 5.5, 6.8, and 7.4).

DOX release from ReS2@mSiO2-RhB reached a cumulative average of 25.1% after 12 h. However, in the acidic environment of pH 5.5 and the weakly acidic environment of pH 6.8, an average of 96.2% and 57.8% DOX can be released respectively within 12 h (cumulative), demonstrating that the release of DOX from ReS₂@mSiO₂-RhB-DOX is pHdependent.³² This observed trend is in agreement with other literature reports; 33 the p K_a of the DOX amino group is 8.2 and that of silanol groups of mesoporous silica is \sim 3.5, hence, at pH 7.4, DOX is partially positively charged, and the silanol groups are deprotonated, thus both remaining electrostatically attracted. Below pH 7.4 the silanol groups as well as DOX amino groups become partially protonated, resulting in repulsive interactions that lead to the release of DOX.³³ The results confirmed that ReS2@mSiO2-RhB can serve as a drug carrier sensitive to acidic endosomes and lysosomal pH for efficient drug release in tumor cells.

3.6. Combined Anticancer Therapy *In Vitro*. Based on the above photothermal and drug release results, the cell viability of different groups was tested in HeLa cells (Figure 5). We found that ReS₂@mSiO₂-RhB has a minimal killing effect on normal cells, with 80% cell viability in the ReS₂@mSiO₂-RhB group as a result of the CCK-8 cytotoxicity evaluation. After being irradiated with the 808 nm laser for 10 min, the cell

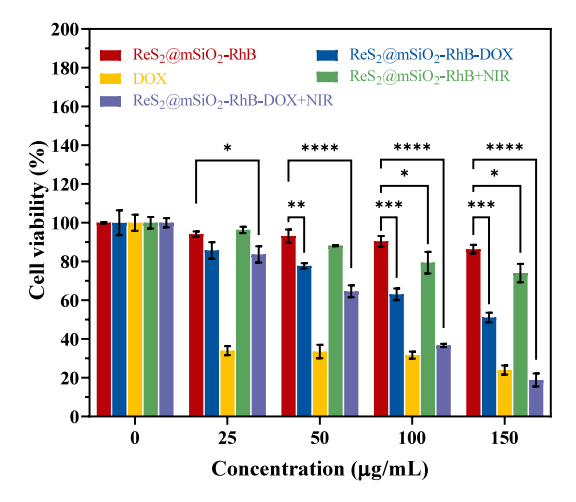


Figure 5. Cell viability of HeLa cells treated with different concentrations of ReS₂@mSiO₂-RhB, ReS₂@mSiO₂-RhB-DOX, DOX, ReS₂@mSiO₂-RhB + NIR, and ReS₂@mSiO₂-RhB-DOX + NIR, respectively.

viability in the ReS₂@mSiO₂-RhB + NIR group decreased with increasing nanosphere concentration, attributed to the photothermal performance of ReS2@mSiO2-RhB itself. For the ReS₂@mSiO₂-RhB-DOX group, there is an obvious killing effect with increasing concentration, which was attributed to the killing effect of DOX released by ReS2@mSiO2-RhB on cells. After being irradiated with the 808 nm laser for 10 min, the cell viability in the ReS₂@mSiO₂-RhB-DOX + NIR group significantly decreased, representing the highest antitumor efficiency when compared with other groups at the same drug concentration after 24 h of incubation. DOX is known to cause cardiotoxicity in the body leading to heart failure, so it is administered systemically.³⁴ Thus, the above results suggest that ReS2@mSiO2-RhB nanoparticle administration directly to the tumor combined with PTT could have safe and efficient antitumor effects in vivo.

In addition, the cell-killing effect was directly observed by conducting green nucleic acid staining via CLSM after different treatments. A green fluorescence dye, BD Via-Probe Green, was used to stain living cells. The ReS₂@mSiO₂-RhB nanoparticles labeled with the Rhodamine B probe exhibit red fluorescence, enabling the observation of the hybrid material colocalization with the cells.

HeLa cells were divided into six groups: (1) PBS; (2) PBS + NIR; (3) ReS₂@mSiO₂-RhB; (4) ReS₂@mSiO₂-RhB + NIR; (5) ReS₂@mSiO₂-RhB-DOX; and (6) ReS₂@mSiO₂-RhB-DOX + NIR. (Figure 6). The first group was set up as the negative control. Since the cells only received 808 nm laser irradiation in group 2, the number of viable cells was not significantly reduced, indicating a small side effect of the 808 nm laser on HeLa cells. In group 3, slight toxicity of ReS₂@ mSiO₂-RhB was observed, consistent with the CCK-8 cytotoxicity and cell viability evaluation. In group 4, the number of viable cells was significantly reduced, following the increasing ReS2@mSiO2-RhB inside the cells, and the green fluorescence intensity was significantly weakened, indicating that after laser irradiation, the cell viability of HeLa cells was weakened due to high temperature, which potentially increased cell membrane permeability. In group 5, ReS₂@mSiO₂-RhB was located in close proximity to the cell nucleus; the cell morphology changed, the number of cells decreased, and the green fluorescence intensity was significantly weakened,

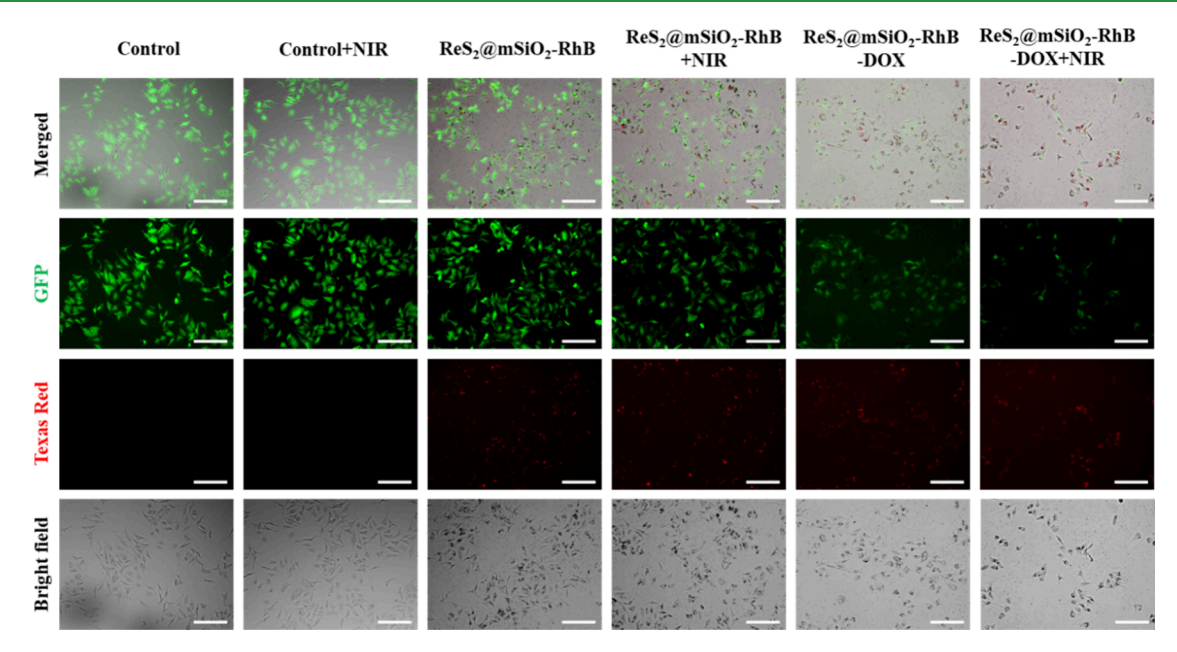


Figure 6. Fluorescence images of HeLa cells treated with PBS, PBS + NIR, ReS₂@mSiO₂-RhB, ReS₂@mSiO₂-RhB + NIR, ReS₂@mSiO₂-RhB-DOX, and ReS₂@mSiO₂-RhB-DOX + NIR, respectively. Scale bars: 200 nm.

indicating that ReS₂@mSiO₂-RhB-DOX has the best chemotherapeutic effect. After irradiation in the last group, the cell morphology changed significantly and the green fluorescence signal virtually disappeared. These results further confirmed that ReS₂@mSiO₂-RhB could effectively kill HeLa cells through combined chemotherapy and photothermal therapy.

3.7. Intracellular Uptake. BioTEM was employed to study the intracellular uptake of individual nanoparticles (Figure 7). According to imaging, nanoparticles mainly

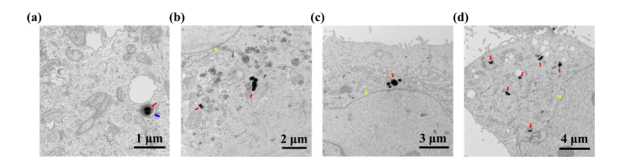


Figure 7. (a–d) BioTEM images of HeLa cells incubated with 100 μ g/mL of ReS₂@mSiO₂-RhB-DOX after 10 min of NIR irradiation, where red arrows show the ReS₂@mSiO₂-RhB-DOX nanoparticles, yellow arrows show the nucleus, and the blue arrow points to the endosome.

accumulate in endosomes or lysosomes in the cytoplasm through endocytosis (Figure 7a). Nanoparticles are located around the cell nucleus without entering the nucleus (Figures 7b–7d). This is consistent with reports indicating that nanoparticles with diameters exceeding 100 nm are unlikely to penetrate the nuclear membrane. The ReS₂@mSiO₂-RhB-DOX could also escape from endosomes and enter the cytoplasm via a cellular "sponge effect". It is important to note that the internalized nanoparticles maintained their structural integrity (Figure 6d).

4. CONCLUSION

An inorganic—inorganic core—shell hybrid nanoplatform for combined chemo-photothermal therapy was developed by encapsulating ReS_2 in a mesoporous silica shell. The design involves ReS_2 as a photothermal agent and mesoporous silica drug delivery carrier. The silica shell precursors were

engineered to covalently attach a fluorescent dye, thus conferring overall imaging capabilities to the nanocarrier. Doxorubicin was used as a proof-of-concept drug for demonstrating drug loading and release of ReS2@mSiO2-RhB. The pH-responsive drug delivery was demonstrated by testing the carrier in HeLa cells, where the acidic environment of cancer cells triggered the breakage of hydrogen bonds between silica and the drug. Upon subjecting the nanoparticles to NIR by irradiation with an 808 nm laser, the temperature around the nanoparticles increases by transferring light to heat, thereby killing cancer cells. ReS2@mSiO2-RhB has demonstrated good biocompatibility when the concentration is <100 μg/mL. In vitro tests also showed that ReS₂@mSiO₂-RhB-DOX can be efficiently internalized into HeLa cells. Importantly, the in vitro study demonstrated remarkable anticancer performance of the combination of chemo/PTT. In vitro studies demonstrated that the drug loaded nanoparticles ReS₂@mSiO₂-RhB-DOX were efficiently internalized into HeLa cells. Significant in vitro cell killing was achieved in over 80% of cancer cells killed when chemo/PTT was employed, which is much higher than that of the single chemo of 49% cell killing and the single PTT of 26% cell killing and equivalent to the effect of free high-concentration DOX. These results lay a strong foundation for future in vivo testing.

ASSOCIATED CONTENT

Supporting Information

The Supporting Information is available free of charge at https://pubs.acs.org/doi/10.1021/acsabm.4c00291.

Low-angle XRD patterns of as-ReS₂@mSiO₂-RhB and ReS₂@mSiO₂-RhB; particle size distribution curve of ReS₂; SAED pattern of ReS₂@mSiO₂-RhB; photothermal heating curves of various concentrations and photothermal stability of ReS₂ irradiated by an 808 nm laser; calibration curve of DOX at 480 nm and DOX structure; BET surface area and DFT pore size distribution of ReS₂@mSiO₂-RhB and ReS₂@mSiO₂-

RhB-DOX; SEM images of ReS₂ with various amounts of PVP; UV—vis spectra of ReS₂@mSiO₂-RhB and ReS₂ at various concentrations; calculation of photothermal conversion efficiency; temperature responses of the heating and the cooling period and plots of linear fitting time versus negative natural logarithm of driving force temperature of ReS₂@mSiO₂-RhB at various concentrations; temperature responses of the heating and the cooling period and plots of linear fitting time versus negative natural logarithm of driving force temperature of ReS₂ at various concentrations; and electron microscopy sample preparation for cells (PDF)

AUTHOR INFORMATION

Corresponding Author

Cheng-Yu Lai — Department of Mechanical and Materials Engineering, Florida International University, Miami, Florida 33174, United States; Department of Chemistry and Biochemistry, Florida International University, Miami, Florida 33199, United States; ⊙ orcid.org/0000-0002-8931-5601; Email: clai@fiu.edu

Authors

Ha Na − Department of Mechanical and Materials Engineering, Florida International University, Miami, Florida 33174, United States; orcid.org/0000-0003-0872-7231

Jake Carrier – Department of Chemistry and Biochemistry, Florida International University, Miami, Florida 33199, United States

Samuel Oyon — Department of Mechanical and Materials Engineering, Florida International University, Miami, Florida 33174, United States; orcid.org/0009-0008-4519-663X

Complete contact information is available at: https://pubs.acs.org/10.1021/acsabm.4c00291

Author Contributions

The manuscript was written through the contributions of all authors. All authors have given approval to the final version of the manuscript.

Notes

The authors declare no competing financial interest.

ACKNOWLEDGMENTS

This work was supported in part by the NSF Award DMR-2122078, the NASA Award 80NSSC19M0201, and DoD Awards W911NF2310152 and W911NF2210186. J.C. acknowledges support from the FIU Veteran Fellowship awarded by the FIU Graduate School. The authors thank Dr. Daniela Radu at Florida International University for valuable suggestions to authors during manuscript preparation. S.O. acknowledges support by the NSF FGLSAMP FIU Bridge to the Doctorate Award HRD #2204743. The authors thank Ms. Shannon Modla of Delaware Biosciences Institute for BioTEM. The BioTEM microscopy ThermoFisher Talos/F200X equipment was procured with NIH-NIGMS (P20 GM103446) and the Unidel Foundation, and access was supported by NIGMS (P20 GM139760) and the State of Delaware.

■ REFERENCES

(1) Debela, D. T.; Muzazu, S. G.; Heraro, K. D.; Ndalama, M. T.; Mesele, B. W.; Haile, D. C.; Kitui, S. K.; Manyazewal, T. New

- approaches and procedures for cancer treatment: Current perspectives. SAGE Open Med. 2021, 9, 205031212110343.
- (2) Huang, L.; Zhao, S.; Fang, F.; Xu, T.; Lan, M.; Zhang, J. Advances and perspectives in carrier-free nanodrugs for cancer chemo-monotherapy and combination therapy. *Biomaterials* **2021**, 268, 120557.
- (3) Cheng, W.; Nie, J.; Gao, N.; Liu, G.; Tao, W.; Xiao, X.; Jiang, L.; Liu, Z.; Zeng, X.; Mei, L. A Multifunctional Nanoplatform against Multidrug Resistant Cancer: Merging the Best of Targeted Chemo/Gene/Photothermal Therapy. *Adv. Funct. Mater.* **2017**, 27 (45), 1704135.
- (4) Fernandes, N.; Rodrigues, C. F.; Moreira, A. F.; Correia, I. J. Overview of the application of inorganic nanomaterials in cancer photothermal therapy. *Biomaterials science* **2020**, *8* (11), 2990–3020.
- (5) Yao, Y.; Zhou, Y.; Liu, L.; Xu, Y.; Chen, Q.; Wang, Y.; Wu, S.; Deng, Y.; Zhang, J.; Shao, A. Nanoparticle-Based Drug Delivery in Cancer Therapy and Its Role in Overcoming Drug Resistance. *Front Mol. Biosci* **2020**, *7*, 193.
- (6) Huang, X.; El-Sayed, M. A. Gold nanoparticles: Optical properties and implementations in cancer diagnosis and photothermal therapy. *Journal of advanced research* **2010**, *1* (1), 13–28.
- (7) Zhou, Z.; Sun, Y.; Shen, J.; Wei, J.; Yu, C.; Kong, B.; Liu, W.; Yang, H.; Yang, S.; Wang, W. Iron/iron oxide core/shell nanoparticles for magnetic targeting MRI and near-infrared photothermal therapy. *Biomaterials* **2014**, *35* (26), 7470–7478.
- (8) Li, K.-C.; Chu, H.-C.; Lin, Y.; Tuan, H.-Y.; Hu, Y.-C. PEGylated copper nanowires as a novel photothermal therapy agent. *ACS Appl. Mater. Interfaces* **2016**, 8 (19), 12082–12090.
- (9) Zhou, Z.; Kong, B.; Yu, C.; Shi, X.; Wang, M.; Liu, W.; Sun, Y.; Zhang, Y.; Yang, H.; Yang, S. Tungsten oxide nanorods: an efficient nanoplatform for tumor CT imaging and photothermal therapy. *Sci. Rep.* **2014**, *4* (1), 3653.
- (10) Zhan, Y.; Liu, Y.; Zu, H.; Guo, Y.; Wu, S.; Yang, H.; Liu, Z.; Lei, B.; Zhuang, J.; Zhang, X.; et al. Phase-controlled synthesis of molybdenum oxide nanoparticles for surface enhanced Raman scattering and photothermal therapy. *Nanoscale* **2018**, *10* (13), 5997–6004.
- (11) Moon, H. K.; Lee, S. H.; Choi, H. C. In vivo near-infrared mediated tumor destruction by photothermal effect of carbon nanotubes. *ACS Nano* **2009**, 3 (11), 3707–3713.
- (12) Issels, R. D. Hyperthermia adds to chemotherapy. *Eur. J. Cancer* **2008**, 44 (17), 2546–2554.
- (13) Gurunathan, S.; Kang, M. H.; Qasim, M.; Kim, J. H. Nanoparticle-Mediated Combination Therapy: Two-in-One Approach for Cancer. *Int. J. Mol. Sci.* **2018**, *19* (10), 3264.
- (14) Liu, S.; Pan, X.; Liu, H. Two-Dimensional Nanomaterials for Photothermal Therapy. *Angew. Chem., Int. Ed.* **2020**, *59* (15), 5890–5000
- (15) Wu, J.; Hu, T.; Zhao, G.; Li, A.; Liang, R. Two-dimensional transition metal chalcogenide nanomaterials for cancer diagnosis and treatment. *Chin. Chem. Lett.* **2022**, 33 (10), 4437–4448.
- (16) Yang, H.; Zhao, J.; Wu, C.; Ye, C.; Zou, D.; Wang, S. Facile synthesis of colloidal stable MoS2 nanoparticles for combined tumor therapy. *Chemical Engineering Journal* **2018**, 351, 548–558.
- (17) Yang, G.; Gong, H.; Liu, T.; Sun, X.; Cheng, L.; Liu, Z. Two-dimensional magnetic WS2@Fe3O4 nanocomposite with mesoporous silica coating for drug delivery and imaging-guided therapy of cancer. *Biomaterials* **2015**, *60*, 62–71.
- (18) Wang, X.; Wang, J.; Pan, J.; Zhao, F.; Kan, D.; Cheng, R.; Zhang, X.; Sun, S.-K. Rhenium Sulfide Nanoparticles as a Biosafe Spectral CT Contrast Agent for Gastrointestinal Tract Imaging and Tumor Theranostics in Vivo. ACS Appl. Mater. Interfaces 2019, 11 (37), 33650–33658.
- (19) Miao, Z.-H.; Lv, L.-X.; Li, K.; Liu, P.-Y.; Li, Z.; Yang, H.; Zhao, Q.; Chang, M.; Zhen, L.; Xu, C.-Y. Liquid Exfoliation of Colloidal Rhenium Disulfide Nanosheets as a Multifunctional Theranostic Agent for In Vivo Photoacoustic/CT Imaging and Photothermal Therapy. *Small* **2018**, *14* (14), 1703789.

- (20) Liu, S.; Lei, W.; Liu, Y.; Zhang, W.-H. Uniform ReS2 porous nanospheres assembled from curly ReS2 few-layers with an expanded interlayer spacing for high-performance lithium-ion batteries. *Chemical Engineering Journal* **2019**, 357, 112–119.
- (21) Lai, C.-Y.; Wu, C.-W.; Radu, D.; Trewyn, B.; Lin, V.-Y. Reversible binding and fluorescence energy transfer between surface-derivatized CdS nanoparticles and multi-functionalized fluorescent mesoporous silica nanospheres. In *Studies in Surface Science and Catalysis*, Vol. 170; Elsevier, 2007; pp 1827–1835.
- (22) Deng, Y.; Qi, D.; Deng, C.; Zhang, X.; Zhao, D. Superparamagnetic High-Magnetization Microspheres with an Fe3O4@ SiO2 Core and Perpendicularly Aligned Mesoporous SiO2 Shell for Removal of Microcystins. J. Am. Chem. Soc. 2008, 130 (1), 28–29.
- (23) Na, H.; Venedicto, M.; Chang, C.-Y.; Carrier, J.; Lai, C.-Y. Infrared-Activated Bactericide: Rhenium Disulfide (ReS2)-Functionalized Mesoporous Silica Nanoparticles. *ACS Applied Bio Materials* **2023**, *6* (4), 1577–1585.
- (24) Reddy Inta, H.; Biswas, T.; Ghosh, S.; Kumar, R.; Kanti Jana, S.; Mahalingam, V. Ionic Liquid-Intercalated Metallic MoS2 as a Superior Electrode for Energy Storage Applications. *ChemNanoMat* **2020**, *6* (4), 685–695.
- (25) Su, G.; Yang, C.; Zhu, J.-J. Fabrication of gold nanorods with tunable longitudinal surface plasmon resonance peaks by reductive dopamine. *Langmuir* **2015**, *31* (2), 817–823.
- (26) Bilalis, P.; Tziveleka, L.-A.; Varlas, S.; Iatrou, H. pH-Sensitive nanogates based on poly(l-histidine) for controlled drug release from mesoporous silica nanoparticles. *Polym. Chem.* **2016**, *7* (7), 1475–1485.
- (27) Raval, N.; Maheshwari, R.; Kalyane, D.; Youngren-Ortiz, S. R.; Chougule, M. B.; Tekade, R. K. Importance of Physicochemical Characterization of Nanoparticles in Pharmaceutical Product Development. In *Basic Fundamentals of Drug Delivery*, Tekade, R. K., Ed.; Academic Press, 2019; pp 369–400.
- (28) Zhang, S.; Chowdari, B. V. R.; Wen, Z.; Jin, J.; Yang, J. Constructing Highly Oriented Configuration by Few-Layer MoS2: Toward High-Performance Lithium-Ion Batteries and Hydrogen Evolution Reactions. ACS Nano 2015, 9 (12), 12464–12472.
- (29) Majumder, S.; Banerjee, S. Flower-Like MoS2 for Next-Generation High-Performance Energy Storage Device Applications. *Microscopy and Microanalysis* **2019**, 25 (6), 1394–1400.
- (30) Baldovino-Medrano, V. G.; Niño-Celis, V.; Isaacs Giraldo, R. Systematic Analysis of the Nitrogen Adsorption-Desorption Isotherms Recorded for a Series of Materials Based on Microporous-Mesoporous Amorphous Aluminosilicates Using Classical Methods. *Journal of Chemical & Engineering Data* 2023, 68 (9), 2512–2528.
- (31) Ding, J.; Xiao, C.; Li, Y.; Cheng, Y.; Wang, N.; He, C.; Zhuang, X.; Zhu, X.; Chen, X. Efficacious hepatoma-targeted nanomedicine self-assembled from galactopeptide and doxorubicin driven by two-stage physical interactions. *J. Controlled Release* **2013**, *169* (3), 193–203.
- (32) Hu, Z.; Xu, C.; Liang, Y.; Liu, T.; Tian, H.; Zhang, Y. Multifunctional drug delivery nanoparticles based on MIL-100 (Fe) for photoacoustic imaging-guided synergistic chemodynamic/chemo/photothermal breast cancer therapy. *Materials & Design* **2022**, 223, 111132.
- (33) Gisbert-Garzaran, M.; Manzano, M.; Vallet-Regi, M. pH-Responsive Mesoporous Silica and Carbon Nanoparticles for Drug Delivery. *Bioengineering (Basel)* **2017**, *4* (1), 3.
- (34) Rawat, P. S.; Jaiswal, A.; Khurana, A.; Bhatti, J. S.; Navik, U. Doxorubicin-induced cardiotoxicity: An update on the molecular mechanism and novel therapeutic strategies for effective management. *Biomedicine & Pharmacotherapy* **2021**, *139*, 111708.
- (35) Llinàs, M. C.; Martínez-Edo, G.; Cascante, A.; Porcar, I.; Borrós, S.; Sánchez-García, D. Preparation of a mesoporous silicabased nano-vehicle for dual DOX/CPT pH-triggered delivery. *Drug delivery* **2018**, 25 (1), 1137–1146.